CrystEngComm

PAPER

Cite this: *CrystEngComm*, 2016, **18**, 8953

The supramolecular effect of aromaticity on the crystal packing of furan/thiophene carboxamide compounds†

M. Rahmani,[a] A. Salimi,*[a] S. Mohammadzadeh[a] and H. A. Sparkes[b]

Received 6th September 2016,
Accepted 24th October 2016

DOI: 10.1039/c6ce01945e

www.rsc.org/crystengcomm

N-2-pyrazinyl-2-furancarboxamide (I) and *N*-2-pyrazinyl-2-thiophenecarboxamide (II) are compounds containing different five-membered heteroaromatic rings, furan and thiophene, respectively. They were designed and synthesized to examine the effect of an increase in aromaticity from furan to thiophene on the crystal packing. In order to explore the various features of the crystal packing motifs in more detail, single crystal X-ray diffraction, Hirshfeld surface analysis and theoretical calculations were carried out on the two compounds. The results clearly show that the heteroatom substitution of O to S in five-membered rings led to an increase in the effectiveness of π-based interactions in II, whereas hydrogen bond interactions play a more important role in the stabilization of the supramolecular architecture of I.

Introduction

Knowledge-based selection of building blocks that participate in creating specific molecular structures and intermolecular interactions in crystal structures are essential pillars in supramolecular chemistry.[1] Obviously, the best choice of building block can act as a directing agent to determine the type of interactions as well as providing the possibility of cooperative interactions in order to create a stable supramolecular network.[2] The field of crystal engineering relies on considerable efforts to understand, control and predict the interaction behavior and crystal packing of specific building blocks in order to control and design specific properties into a molecular solid.[3]

In this regard, aromatic structural units (such as six-membered or five-membered heteroaromatic rings) which can be engaged in various hydrogen bonding and especially π-based interactions have been widely investigated by experimental and theoretical studies.[4] In particular, many research groups have studied the five-membered heteroaromatic systems in terms of various molecular properties such as their geometric, electronic,[5] energetic,[6] or magnetic properties as well as aromaticity levels.[7] The aromaticity level is one of the most important properties which has a dominant role in π-based interactions and therefore its quantification can be a valuable feature in the assessment of the likely strength and interaction nature from a crystal engineering viewpoint. In this regard, a lot of theoretical and experimental methods have been developed in order to provide a quantitative measurement of aromaticity according to various criteria, namely, geometrical, energetic, magnetism, electronic and reactivity-based indices.[8]

Studies on the aromaticity of the five-membered heteroaromatic rings indicated that their aromaticity increases in the order of furan, pyrrole, thiophene.[9,10] In this series, furan and thiophene with minimum and maximum aromatic levels, respectively, can serve as good candidates to explore the effect of changes in aromaticity on the π-based interactions as well as various hydrogen bonding through O and S acceptors. It should be noted that these interactions can play different roles in the crystal packing so that some of them may be important factors in the stability of packing structures. The cooperative effects within these interactions (especially weak intermolecular interactions) can also be important in the self-assembly process of molecular structures containing these aromatic systems. Therefore, an understanding of the intermolecular forces within the structures is essential to provide insights into the interaction behavior of a particular system. Nowadays, a significant number of theoretical and experimental studies have been focused on this issue for controlling self-assembly and molecular packing.[11–13]

Herein, we report the crystal structures and computational results of two pyrazine amide compounds, *N*-2-pyrazinyl-2-furancarboxamide (**I**) and *N*-2-pyrazinyl-2-thiophenecarboxamide (**II**) containing three moieties of a

[a] *Department of Chemistry, Ferdowsi University of Mashhad, 917791436, Mashhad, Iran. E-mail: salimi-a@um.ac.ir*
[b] *School of Chemistry, University of Bristol, Cantock's Close, Bristol, BS8 1TS, UK*

† Electronic supplementary information (ESI) available: Additional structural data, Cambridge Structural Database (CSD) analysis, histograms and scattergrams, NMR and IR data, and computationally binding energies of tetramer fragments. CCDC 1415044 and 1415045 contain the supplementary crystallographic data for this paper. For ESI and crystallographic data in CIF or other electronic format see DOI: 10.1039/c6ce01945e

pyrazine ring (Pyz), an amide group (NHCO) and a five-membered heteroaromatic ring, furan or thiophene, respectively (Fig. 1). More importantly, we realized the effect of the level of aromaticity of furan and thiophene on directing the supramolecular interactions and modulating the H-bonding and π-stacking in the assembly process. Comparison of related crystal packing, DFT computation of binding energies of various non-covalent motifs and Hirshfeld surface analysis[14] were performed to identify the preferred supramolecular synthons in **I** and **II**. The aromaticity level of the five-membered heteroaromatic rings measured by using a harmonic oscillator model of aromaticity (HOMA) as a geometrical-based index and the arrangement of these moieties in the crystal packing structures were examined in detail.

Experimental section

All the reagents and solvents for syntheses and analyses were purchased from Aldrich or Merck and used without further purification. The synthesis and recrystallization of compounds **I** and **II** were carried out in air. The ^{1}H and ^{13}C NMR spectra were recorded on a Bruker AC-400 MHz spectrometer at ambient temperature in $CDCl_3$. The coupling constants were reported in Hertz. The infrared spectra (4000–250 cm^{-1}) of the solid sample were taken as 1% dispersion in KBr pellets using a BOMEM-MB102 spectrometer. Elemental analysis was performed using a Heraeus CHN-O Rapid analyzer. Melting point was obtained by using a Barnstead Electrothermal type 9200 melting point apparatus and was corrected. NMR and IR characterization data are provided in the ESI.†

X-ray diffraction experiments on compounds **I** and **II** were carried out at 120 K using an Agilent SuperNova Dual Source diffractometer with Mo-K_α radiation (λ = 0.71073 Å). Data collections were performed using a CCD area detector from a single crystal mounted on a glass fiber. Intensities were integrated and absorption corrections were applied using CrysAlisPro software version 1.171.36.28.[15] Both structures were solved using olex2.solve,[16] and all of the structures were refined against F^2 in SHELXL[17] using Olex2.[18] All of the non-hydrogen atoms were refined anisotropically, while all of the hydrogen atoms were located geometrically and refined using a riding model. The crystal structure and refinement data are given in Table 1.

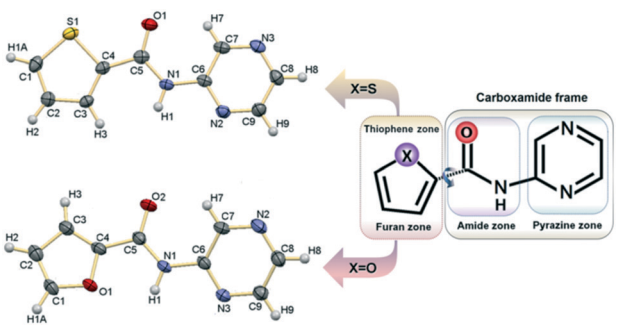

Fig. 1 Representation of the different regions of the designed compounds, **I** and **II** (right). Molecular structures of **I** and **II** with the thermal ellipsoids at the 30% probability level. The H atoms are of arbitrary size (left).

Synthesis of compound I

A solution of 10.0 mmol of furan-2-carboxylic acid (1.12 g) in 10.0 mL of pyridine was added to a solution 10.0 mmol of 2-aminopyrazine (0.95 g) in 10.0 mL of pyridine. The resulting solution was stirred at 313 K for 20 min, then 10.0 mmol of triphenyl phosphite (2.76 mL) was added dropwise, and the reaction mixture was stirred at 373 K for 2 h and at ambient temperature for 5 h. The amide product was filtered as a white powder (75% yield). Upon slow evaporation of the filtrate at room temperature, colorless needle shaped crystals for compound **I** suitable for X-ray analysis were obtained after 13 days. Mp: 172–173 °C. Anal calcd for $C_9H_7N_3O_2$: C: 57.14, H: 3.73, N: 22.21%; found: C: 57.16, H: 3.50, N: 22.25%.

Synthesis of compound II

A solution with a 1 : 1 molar ratio of 2-aminopyrazine (10.0 mmol, 0.951 g) and thiophene-2-carboxylic acid chloride (10.0 mmol, 1.07 mL) in 10.0 mL of dry pyridine was produced. The resulting solution was stirred at ambient temperature for 1 h. A transparent solution resulted which was then filtered. X-ray quality colorless cubic crystals were harvested by slow solvent evaporation at room temperature for 10 days with a yield of 27%. Mp: 122–123 °C. Anal calcd for $C_9H_7N_3OS$: C: 52.67, H: 3.44, N: 20.47, S: 15.62%; found: C: 52.45, H: 3.52, N: 20.26, S: 15.38%.

Computational methods

The most stable (probable) *syn* and *anti*-conformations for each of the title compounds were obtained *via* full optimization using DFT calculations (the B3LYP method with the

Table 1 Structural data and refinement for compounds **I** and **II**

	I	**II**
Empirical formula	$C_9H_7N_3O_2$	$C_9H_7N_3OS$
Formula weight	189.18	205.24
Temperature/K	120(2)	120(2)
Crystal system	Orthorhombic	Monoclinic
Space group	*Fdd*2	$P2_1/n$
a/Å	30.656(3)	7.9507(4)
b/Å	27.727(5)	11.7608(5)
c/Å	3.7908(4)	10.1981(4)
α/°	90	90
β/°	90	110.216(5)
γ/°	90	90
Volume/Å^3	3222.2(7)	894.84(7)
Z	16	4
ρ_{calc}/g cm^{-3}	1.560	1.523
μ/mm^{-1}	0.115	0.327
F(000)	1568.0	424.0
Reflections collected	7656	4546
Data/restraints/parameters	1861/1/127	2091/0/127
Goodness-of-fit on F^2	1.074	1.075
R_1, wR_2 for data $I > 2\sigma(I)$	0.0499, 0.1221	0.0312, 0.0771
R_1, wR_2 for all data	0.0566, 0.1282	0.0339, 0.0787
Largest diff. peak/hole/e Å^{-3}	0.26/−0.31	0.34/−0.30

6-311+G(d,p) basis set) without any restriction condition, and the frequency analysis showed the absence of imaginary frequencies in any state. The binding energies of all molecular pairs (dimer) were calculated based on M06-2X and M06 (ref. 19) and B3LYP-D3 as a DFT dispersion-corrected method[20] along with the 6-311+G(d,p) basis set to investigate the energy of the non-covalent interactions involved in the supramolecular architectures of the title compounds. Since the calculation of non-covalent interactions from the new DFT-D3 method is particularly reliable where the dispersion component has a significant contribution,[20c] the interaction energies of reasonable double pairs or quaternary fragments (tetramer) were calculated based on the B3LYP-D3 method. The corrections for basis set substitution error (BSSE) were performed using the counterpoise method.[21] We have taken the fragment structural coordinates directly from the crystal structure data with H atoms at their neutron distances (1.08 Å for C–H and 1.00 Å for N–H) as input geometries in the single point energy calculations. All the calculations were performed using the GAMESS program package.[22]

In this study, the electrostatic surface potential (ESP) for individual molecules was mapped on the Hirshfeld surface over the range of −0.015 au (red), through 0 (white), to 0.015 au (blue). For this purpose, *ab initio* wave functions were obtained by using the B3LYP method and the 6-31G(d,p) basis set. The molecular Hirshfeld surfaces[23] presented in this paper were generated using Crystal Explorer 3.1.[24]

Results and discussion

Crystal structure description

Compound **I** crystallizes in the orthorhombic space group *Fdd*2 with one independent molecule in the asymmetric unit (Z = 16, see Table 1). Due to the limited flexibility of **I**, a plate structure is predictable but the twist angle between planes calculated through the two rings is 24.8(1)°, illustrating a curved-like structure. In this structure, the molecules pack to form the variable intermolecular interactions, such as N–H···N, C–H···N, C–H···O, C–H···π and π–π stacking interactions (Fig. 2 and Table 2). The N1–H1···N3 hydrogen bond (HB) forms a stable classical HB-based molecular pair (the $R_2^2(8)$ graph set with a *head-to-tail* configuration) and it can be considered as suitable repetitive species in the crystal packing (Fig. 2, upper right). In this pair, there are also two weak C–H···O hydrogen bonds between the C9–H9 of the pyrazine ring and the oxygen atom of the furan ring *via* the formation of the $R_2^2(16)$ pattern. The repetition of the main fragment accompanied by C–H···N/C–H···O hydrogen bonds (C3–H3···N2(pyz) and C8–H8···O2(amide) with the $R_2^2(8)$ graph set) develops 2D supramolecular sheets along the *ab*-plane (Fig. 2, bottom). Additional reinforcement between molecules in the sheet is provided by the C1–H1A···O2(amide) (Fig. 2, right) and the C2–H2···N2(pyz) (Fig. 2, left) hydrogen bonds. Consequently, the sheets are packed *via* C–H···π and π···π stacking interactions in the *c*-direction to create a three-dimensional architecture.

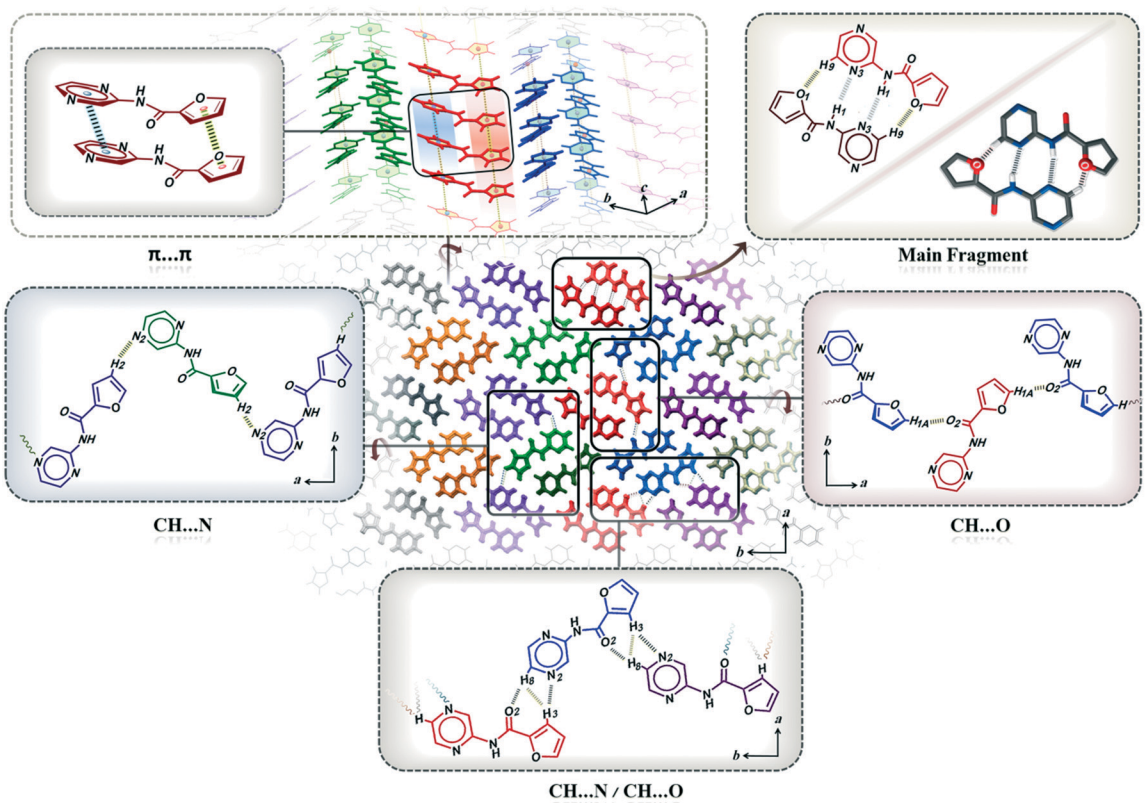

Fig. 2 A representation of part of the unit cell contents of **I**, viewed in various projections. Different colors are shown for different dimer motifs for clarity of various intermolecular interactions.

Table 2 Experimental (X-ray) geometrical parameters of interactions involved in all molecular pairs of compounds **I** and **II** and the binding energies calculated at the DFT-D, M06-2X and M06 methods (dimers were labeled based on the energy relevance)

Molecular pair no.	Symmetry code	Involved interactions	X-ray geometry[a] (Å, deg)	Binding energy, E_{calc} (kJ mol^{-1})		
				DFT-D	M06-2X	M06
Compound **I**						
D1(HB)	1/2 − *x*, 1/2 − *y*, *z*	N1–H1⋯N3	2.266(2)/3.117(3)/163	−44.20	−37.87	−35.03
		C9–H9⋯O1	2.480(2)/3.011(2)/115			
D2(π⋯π)	*x*, *y*, −1 + *z*	$\pi_{furan}\cdots\pi_{furan}$	3.791(2)/27.32/0.00	−28.04	−29.51	−23.88
		$\pi_{pyz}\cdots\pi_{pyz}$	3.791(2)/27.32/0.00			
D3(HB)	1/4 − *x*, −1/4 + *y*, −1/4 + *z*	C3–H3⋯N2	2.831(2)/3.763(3)/167	−19.88	−15.68	−14.80
		C8–H8⋯O2	2.673(2)/3.575(2)/159			
D4(HB)	−1/4 + *x*, 1/4 − *y*, −1/4 + *z*	C1–H1A⋯O2	2.623(2)/3.537(3)/161	−13.76	−10.84	−10.03
D5(HB)	1/4 + *x*, 1/4 − *y*, −3/4 + *z*	C2–H2⋯N2	2.696(2)/3.350(3)/126	−13.75	−10.64	−9.93
D6(HB)	1/4 − *x*, 1/4 + *y*, 1/4 + *z*	C8–H8⋯O2	2.786(2)/3.211(2)/108	−11.40	−8.81	−8.66
D7(HB)	1/2 − *x*, 1/2 − *y*, 1 + *z*	C9–H9⋯π_{Pyz}	2.964(3)/2.436(2)/159	−7.31	−2.61	−1.50
D8(HB)	1/2 − *x*, −*y*, −1/2 + *z*	C2–H2⋯π_{Pyz}	3.515(3)/2.567(2)/144	−5.76	−3.22	−2.94
Compound **II**						
D1(π⋯π)	1 − *x*, 1 − *y*, −*z*	$\pi_{thio}\cdots\pi_{pyz}$	3.488(3)/18.79/7	−39.44	−34.32	−30.21
D2(HB)	1/2 + *x*, 1/2 − *y*, 1/2 + *z*	N1–H1⋯N3	2.193(2)/3.055(2)/166	−32.08	−24.98	−22.43
		C3–H3⋯N3	2.445(2)/3.350(3)/159			
D3(π⋯π)	−*x*, 1 − *y*, −*z*	$\pi_{thio}\cdots\pi_{thio}$	3.579(3)/18.09/0.00	−27.38	−24.17	−20.08
D4(HB)	1/2 − *x*, 1/2 + *y*, 1/2 − *z*	C1–H1A⋯O1	2.452(2)/3.225(3)/138	−15.68	−11.71	−11.80
D5(HB)	1/2 − *x*, −1/2 + *y*, 1/2 − *z*	C8–H8⋯O1	3.221(3)/3.834(3)/124	−13.77	−9.08	−9.21
D6(π⋯π)	1 − *x*, −*y*, −*z*	$\pi_{pyz}\cdots\pi_{pyz}$	4.327(3)/40.83/3	−10.35	−7.39	−5.59
D7(HB)	1/2 − *x*, 1/2 + *y*, −1/2 − *z*	C2–H2⋯N2	2.753(2)/3.496(3)/136	−9.08	−5.26	−3.09
D8(HB)	−1/2 + *x*, 1/2 − *y*, 1/2 + *z*	C9–H9⋯S1	3.144(2)/3.995(3)/150	−6.25	−2.90	−2.86
D9(HB)	−1/2 + *x*, 1.5 − *y*, −1/2 + *z*	C2–H2⋯S1	3.224(3)/4.145(3)/164	−4.55	−1.24	−1.00

[a] Geometrical parameters of the HB: H⋯A/D⋯A/<D–H⋯A, π⋯π stacking: d_{cent}/<cc-p/<p-p, C–H⋯π: $d_{cent}/d_{pln}/\alpha$.

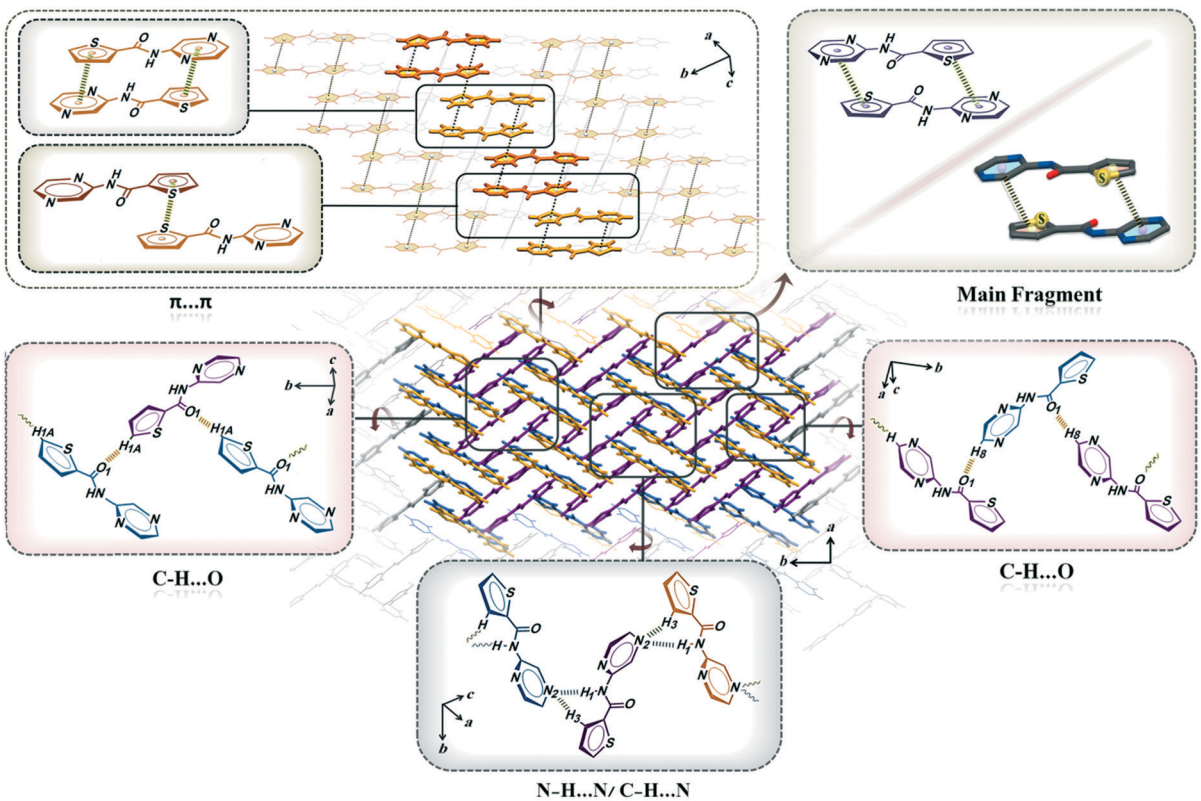

Fig. 3 A representation of part of the unit cell contents of **II** viewed in various projections. Different colors are shown for different dimer motifs for clarity of various intermolecular interactions.

The Cambridge Structural Database (CSD) analysis of C–H···π interactions in a five-membered furan ring reveals that all geometrical parameters of C9–H9···π_{Furan} interactions between adjacent sheets (the H···Cg contact distance and C–H···Cg angle are 2.964 Å and 158.83°, respectively) are in the normal range (for more details, see the ESI†). Moreover, π···π stacking interactions in the form of homosynthons (similar stack rings as $\pi_{Furan}\cdots\pi_{Furan}$ and $\pi_{pyz}\cdots\pi_{pyz}$) happened in the *c*-direction (Fig. 2, upper left and Table 2). A CSD survey for $\pi_{Furan}\cdots\pi_{Furan}$ and $\pi_{pyz}\cdots\pi_{pyz}$ interactions revealed that the parameters associated with **I** all coincide with the maximum frequency of occurrence for such interactions in the CSD (for more details, see the ESI†). Compound **II** crystallizes in the monoclinic space group $P2_1/n$ with $Z = 4$. The angle between the ring planes is 5.35(4)° indicating that the structure is approximately planar. A detailed study of the packing diagram revealed that a 3D supramolecular organic framework structure is formed through complex intermolecular interactions such as N–H···N, C–H···O, C–H···N, C–H···S and π···π interactions (Fig. 3). In this way, one of the major molecular pairs is formed through suitable π···π stacking interactions in which the aromatic rings packed in a *head-to-tail* parallel fashion with a short distance of $\pi_{Thio}\cdots\pi_{Pyz}$ and a limited slippage (Fig. 3, upper right and Table 2). Additionally, the presence of homosynthon $\pi_{Thio}\cdots\pi_{Thio}$ interactions, between thiophene rings in the mentioned adjacent π-based dimer species, leads to stacking of these dimers as 1D tapes in the *ab*-plane (Fig. 3, upper left and Table 2). Our analysis of the CSD for π···π interactions between thiophene rings revealed that the geometrical parameters of this homosynthon lie in a limited number of cases which can be considered as a strong π···π interaction (for more details, see the ESI†).

These results show that there is a strong tendency to form π···π stacking synthons between adjacent aromatic rings, in addition to the N1–H1···N3 classical hydrogen bond (with the C(5) supramolecular synthon), as well as the C3–H3···N3 hydrogen bond (with the $R_2^1(7)$ motif), to further stabilize the packing (Fig. 3, bottom and Table 2). The C–H···O hydrogen bonded synthons (C1–H1A···O1, C8–H8···O1 with the C(6) and C(8) patterns, respectively) cause the expansion of the crystal structure in a three-dimensional architecture (Fig. 3, left and right and Table 2).

Comparison of I and II

The structural definition based on the geometry of aromaticity by numerical identifiers has attracted a lot of attention. In this respect, a measure based on the geometry of the π electron delocalization (aromaticity harmonic oscillator model HOMA) is one of the most effective indexes used to describe the aromaticity.[8a] Therefore, in this work, a detailed study of the local aromaticity was performed using the HOMA indices[25] for the five-membered heterocycle and pyrazine rings which are 0.0911 and 0.9757, respectively, in compound **I**, while the respective values for **II** were 0.8498 and 0.9855. The values indicate that heteroatom substitution from oxygen to sulfur increases the π-electron delocalization level of the five-membered ring, considerably.

The specific consequence of this alteration can be observed in the molecular conformation of title compounds. Obviously, the orientation of furan (O) and thiophene (S) toward the oxygen of the carbonyl group in **I** and **II** (as the *anti* and *syn* conformations, respectively) leads to the presence of N–H···O_{Furan} and lack of significant $S_{Thiophene}$ intramolecular interactions. Reasonably, this evidence can be related to the high localization of electron density (non-bonding pair) on the oxygen heteroatom of the furan ring with a low aromaticity index to participate in the intramolecular hydrogen bonding (and *vice versa* for the aromatic thiophene ring). This progressive withdrawal of the *n*-pair on the heteroatom into the ring from oxygen to sulfur has also been observed in the literature.[26] In order to gain more insight into the stabilization effect of the interamolecular hydrogen bond, two probable conformations (*anti* and *syn*) of each compound were considered theoretically. The full optimization results showed that compound **I** in the *anti*-conformation including an N–H···O interaction is more stable than the *syn* geometry by as much as 15.90 kJ mol^{-1} that is consistent with the experimental structure. On the other hand, the stabilisation energy of the *syn* conformation of **II** is slightly more than the *anti* geometry including the N–H···S interaction (1.34 kJ mol^{-1}). This was confirmed by the geometry of compound **II** from the X-ray structure which showed that the intramolecular interaction of the sulfur atom in the aromatic thiophene ring is not significant enough to be observed in the experimental structure (Fig. S1†).

The electrostatic potential has been mapped over the Hirshfeld surfaces of the title compounds (Fig. 4). A clear separation of the electropositive and electronegative areas was observed over the flat surfaces. However, the electronegative regions on the oxygen atom of the amide group and nitrogen atoms of the pyrazine ring are very similar in two molecules, and there is a significant difference in the electrostatic potential region of the five-membered heteroaromatic rings. Interestingly, the electropositive and

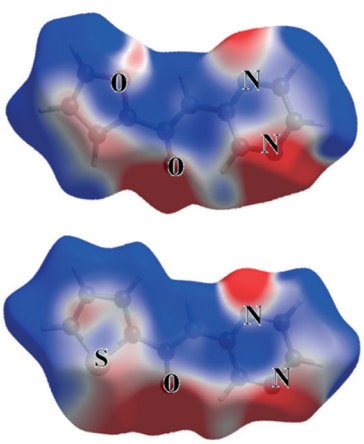

Fig. 4 The Hirshfeld surfaces for **I** and **II** mapped with electrostatic potential (ESP) over the range of −0.015 au (red) through 0.0 (white) to 0.015 au (blue).

electronegative regions on the furan ring show an alternation which is related to the positive and negative charge accumulation on the C1–C4 and C2–C3, O1 atoms, respectively. This issue supports the observation of offset homosynthon $\pi_{Furan}\cdots\pi_{Furan}$ stacking as an electrostatic interaction between these regions (Fig. 2, upper left). Nevertheless, the electronegative region on the thiophene ring is almost uniformly around all atoms, resulting in electrostatic complementarity to the electropositive region on the pyrazine ring, leading to the formation of the significant $\pi_{Thio}\cdots\pi_{Pyz}$ stacking heterosynthon (Fig. 3, upper left). Additionally, the orientation of the ring oxygen and sulfur atoms to the oxygen of the carbonyl group affects the area of the electropositive and electronegative regions on the side of title molecules which have high potential for electrophilic and nucleophilic attack, respectively, in various hydrogen bond interactions in the crystal packing.[27]

It is noteworthy that the privileged formation of the $\pi_{Thio}\cdots\pi_{Pyz}$ interaction in **I** can be also explained based on the "aromatic donor–acceptor" description term suggested by Martinez and Iverson in which stacking between aromatics with differential polarization was described as the interaction of relatively electron-deficient and electron-rich aromatic molecules in an alternating fashion.[4b] In this regard, the pyrazine ring as an electron acceptor and the thiophene ring as a donor group formed this significant interaction.

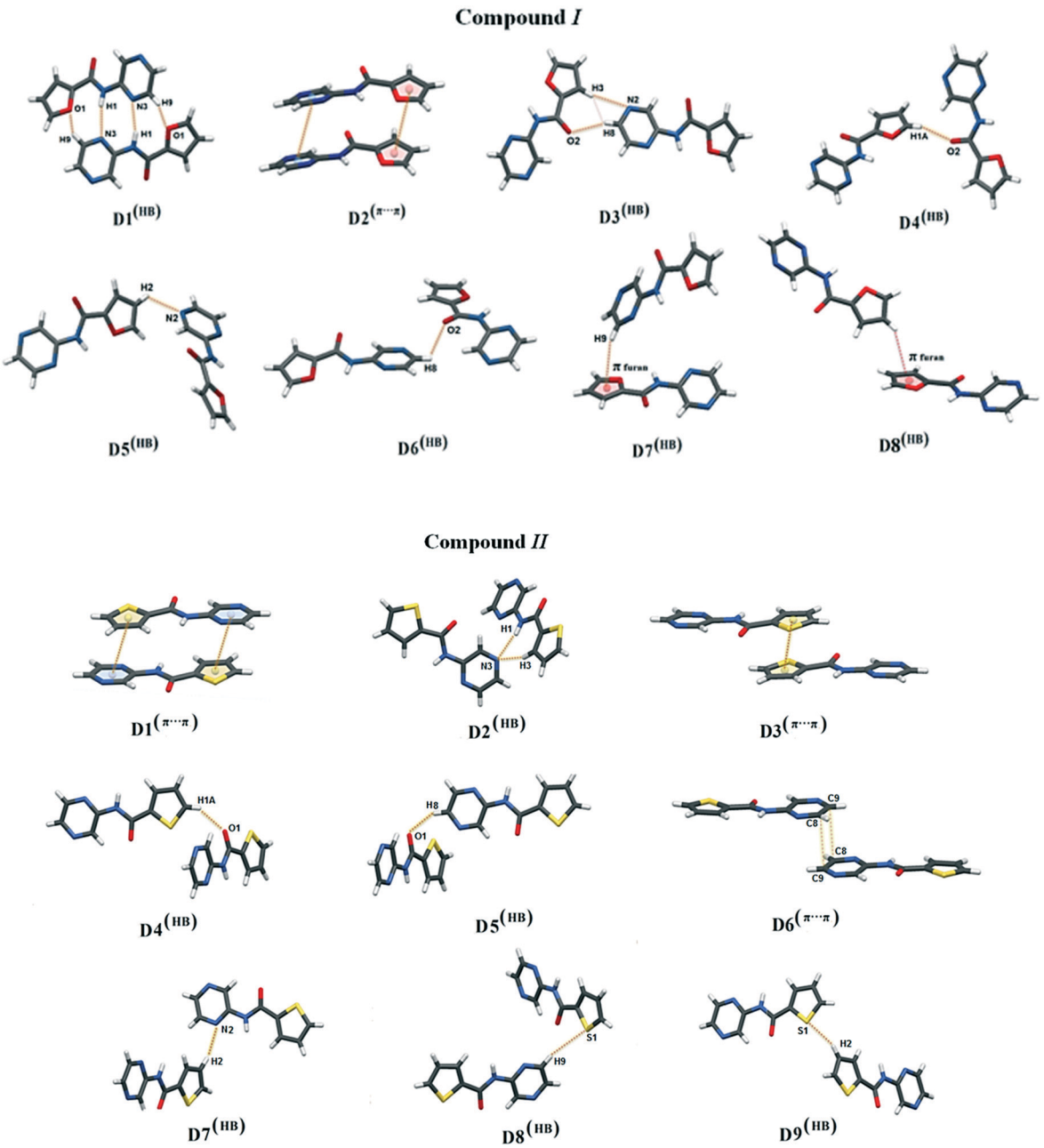

Fig. 5 Stacking patterns observed for all the molecular pairs (dimers) which are labeled based on the interaction energy ranking in **I** and **II**.

Consequently, the more electron donating character of thiophene in comparison to furan revealed the different role of these heteroaromatic rings in the π-based interactions.

In order to gain more insight into the exact effect of the aromaticity level on the crystal packing structures, the cohesive energies of all the molecular pairs (dimer fragments) in the molecular coordination shell of title compounds were calculated and ranked in order of energetic relevance (Fig. 5 and Table 2). The results showed that the supramolecular associations in **I** as dimer species D1 and D3–D8 are based on the hydrogen bond (HB) interactions, whereas D2 is only formed by π···π interactions. Obviously, $D1^{(HB)}$ (IE = −44.20 kJ mol^{-1}) is the most stable molecular pair presented in **I** which is created by the formation of strong N–H···N hydrogen bonds as well as C–H···O interactions (Table 2). The investigation of other dimers showed that $D2^{(\pi\cdots\pi)}$ (IE = −28.04 kJ mol^{-1}) formed *via* homosynthon π···π interactions lies in second place with noticeably lower interaction energy. The other dimers created by the weak hydrogen bonds such as C–H···N and C–H···O synthons showed less stabilisation energies.

On the other hand, the energy ranking in **II** emphasized that the most stable dimer $D1^{(\pi\cdots\pi)}$ (IE = −39.44 kJ mol^{-1}) is created by the formation of two $\pi_{Thio}\cdots\pi_{Pyz}$ heterosynthons. While the second most stable dimeric motif, $D2^{(HB)}$ (IE = −32.09 kJ mol^{-1}), results from directional N–H···N and C–H···N hydrogen bonding, the homosynthon $\pi_{Thio}\cdots\pi_{Thio}$ interaction presented in $D3^{(\pi\cdots\pi)}$ results in strong π···π stacking of as much as −27.38 kJ mol^{-1} per interaction in the crystal packing **II**. The rest of the dimeric motifs in **II** are formed by the various C–H···N, C–H···O and C–H···S interactions.

The binding energies of pairs in **I** and **II** are in the 5–44 and 5–39 kJ mol^{-1} ranges for the B3LYP-D3 method, respectively. M06-2X and M06 quantities are somewhat smaller between 1–37 and 1–34 kJ mol^{-1} for **I** and **II**, respectively. Regarding the presence of multi-interactions in each pair, they are in the normal ranges of HB (*ca.* 1–160 kJ mol^{-1}) and π-stacking (*ca.* 2–50 kJ mol^{-1}) interaction energies.[28]

In light of the dimeric motif binding energies, we have chosen the forty most stable double pairs of compounds **I** and **II** as tetramer fragments (see the ESI†) and calculated the complexation energies to give a relative weight of interaction energies (HB and π stacking) that influence the formation of supramolecular aggregation in the self-assembly processes.

Investigation of these tetramer motifs also provided useful information on the additive and non-additive effects of the HB-bonding and π···π stacking in title structures. In this regard, the magnitude of cooperativity was calculated by deducting all pairwise interactions from the total complexation energy of the tetramer. The total binding energy, the contribution of cooperativity, HB and π···π stacking energies as the magnitude and percentage of total binding energy, as well as the weighted contribution of cooperativity, HB and π···π stacking as a percentage of the overall total binding energies of the studied fragments, and the summation of the weighted contribution of cooperativity, HB and π···π stacking for all of the most stable tetramer fragments of **I** and **II** are shown in Tables S1 and S2,† respectively.

The binding energies range between −51.84 and −160.27 kJ mol^{-1} for **I**. The most stable tetramer fragment of **I** (Tet1) is formed by the participation of strong dimers $D1^{(HB)}$, $D2^{(\pi\cdots\pi)}$ and $D7^{(HB)}$ with an interaction energy of about −160.27 kJ mol^{-1} with additional stability of −1.18 kJ mol^{-1} as an additive effect in this cooperation. The highest cooperativity in the studied complexes of **I** is related to Tet19 in which dimers $D1^{(HB)}$, $D2^{(\pi\cdots\pi)}$ and $D5^{(HB)}$ result in a positive cooperative effect of −4.65 kJ mol^{-1}. Twelve cases of anticooperativity are observed in the range from 0.07 kJ mol^{-1} in Tet37 to 1.45 kJ mol^{-1} in Tet34 of **I**.

The range of total binding energies in the thiophene-based compound is between −46.04 and −140.76 kJ mol^{-1}. Combination of dimers $D1^{(\pi\cdots\pi)}$, $D2^{(HB)}$, $D5^{(HB)}$, $D7^{(HB)}$, and $D9^{(HB)}$ created Tet1 that is first in the tetramer list with the additive effect of −2.39 kJ mol^{-1}. Tet17 containing dimers $D2^{(HB)}$ leads to the highest additive cooperativity of −5.80 kJ mol^{-1}. Additionally, there were 15 cases with a non-additive effect between interactions in which Tet39, formed by π···π based dimers, had the largest negative cooperative effect of 2.31 kJ mol^{-1}.

Regarding the summation of the weighted contribution of HB and π···π stacking interactions in the most stable tetramer fragments, one can conclude that the tendency to form the HB-based molecular pairs (*ca.* 75%) is much higher than π···π stacking motifs (*ca.* 24%) in compound **I** which can be related to the low aromatic index of the furan ring. Although these results emphasized that there is much more tendency to form π-based synthons (*ca.* 49%) based on the aromatic thiophene ring in compound **II**, hydrogen bond interactions still play an important role to stabilize the packing structure.

Conclusions

Two carboxamide compounds containing a furan or a thiophene ring have been synthesized and investigated for the effect of different aromaticity levels of the five-membered ring on supramolecular aggregation using a combination of experimental and computational studies. The energetic study shows that the noncovalent interactions in the molecular pairs (dimer) and doubly pairs (tetramer) are responsible for the supramolecular assemblies observed in the solid state. It is observed that the increase in aromaticity of the thiophene ring in compound **II** encourages to participate in the strong π···π stacking interactions as much as hydrogen bonding. However, this balance significantly changes in favor of strong hydrogen bonding due to the decrease in aromaticity of the furan ring in compound **I**. This study shows that the aromaticity parameter can be utilized as a directing agent to design favorable supramolecular synthons in the context of crystal engineering.

Acknowledgements

The authors gratefully acknowledge the financial support by the Ferdowsi University of Mashhad, Mashhad, Iran (Grant No. 3/25631).

Notes and references

1 (*a*) J.-M. Lehn, *Supramolecular chemistry*, Vch, Weinheim, 1995; (*b*) G. R. Desiraju, *Nature*, 2001, **412**, 397–400; (*c*) J. W. Steed and J. L. Atwood, *Supramolecular chemistry*, John Wiley & Sons, 2013.

2 (*a*) J.-M. Lehn, *Chem. Soc. Rev.*, 2007, **36**, 151–160; (*b*) B. J. Sarmah and D. K. Dutta, *Cryst. Growth Des.*, 2009, **9**, 1643–1645; (*c*) R. Matsidik, J. Martin, S. Schmidt, J. Obermayer, F. Lombeck, F. Nübling, H. Komber, D. Fazzi and M. Sommer, *J. Org. Chem.*, 2015, **80**, 980–987; (*d*) A. Ali, G. Hundal and R. Gupta, *Cryst. Growth Des.*, 2012, **12**, 1308–1319.

3 (*a*) G. R. Desiraju, *J. Am. Chem. Soc.*, 2013, **135**, 9952–9967; (*b*) G. R. Desiraju, J. J. Vittal and A. Ramanan, *Crystal engineering: a textbook*, World Scientific, 2011; (*c*) G. R. Desiraju, *Angew. Chem., Int. Ed.*, 2007, **46**, 8342–8356; (*d*) D. Braga, G. R. Desiraju, J. S. Miller, A. G. Orpen and S. L. Price, *CrystEngComm*, 2002, **4**, 500–509.

4 (*a*) J. I. Wu, J. E. Jackson and P. Schleyer, *J. Am. Chem. Soc.*, 2014, **136**, 13526–13529; (*b*) C. R. Martinez and B. L. Iverson, *Chem. Sci.*, 2012, **3**, 2191–2201; (*c*) H. R. Khavasi and B. Mir Mohammad Sadegh, *Dalton Trans.*, 2015, **44**, 5488–5502; (*d*) H. R. Khavasi and M. Azizpoor Fard, *Cryst. Growth Des.*, 2010, **10**, 1892–1896; (*e*) H. R. Khavasi, A. R. Salimi, H. Eshtiagh-Hosseini and M. M. Amini, *CrystEngComm*, 2011, **13**, 3710–3717; (*f*) H. R. Khavasi and A. Azhdari Tehrani, *Inorg. Chem.*, 2013, **52**, 2891–2905; (*g*) H. R. Khavasi and B. Mir Mohammad Sadegh, *Cryst. Growth Des.*, 2012, **12**, 4798–4804.

5 D. L. Cooper, S. C. Wright, J. Gerratt and M. Raimondi, *J. Chem. Soc., Perkin Trans. 2*, 1989, 263–267.

6 F. Rodríguez-Ropero, J. Casanovas and C. Alemán, *J. Comput. Chem.*, 2008, **29**, 69–78.

7 M. Rosenberg, C. Dahlstrand, K. Kilså and H. Ottosson, *Chem. Rev.*, 2014, **114**, 5379–5425.

8 (*a*) T. M. Krygowski, H. Szatylowicz, O. A. Stasyuk, J. Dominikowska and M. Palusiak, *Chem. Rev.*, 2014, **114**, 6383–6422; (*b*) J.-Y. Sun, L. Wang, D.-J. Zhang, D. Li, Y. Cao, L.-Y. Zhang, S.-L. Zeng, G.-S. Pang, Y. Fan, J.-N. Xu and T.-Y. Song, *CrystEngComm*, 2013, **15**, 3402–3407.

9 K. E. Horner and P. B. Karadakov, *J. Org. Chem.*, 2013, **78**, 8037–8043.

10 K. Najmidin, A. Kerim, P. Abdirishit, H. Kalam and T. Tawar, *J. Mol. Model.*, 2013, **19**, 3529–3535.

11 (*a*) Y. Ma, H. Ma, Z. Yang, J. Ma, Y. Su, W. Li and Z. Lei, *Langmuir*, 2015, **31**, 4916–4923; (*b*) K. B. Bravaya, E. Epifanovsky and A. I. Krylov, *J. Phys. Chem. Lett.*, 2012, **3**, 2726–2732.

12 I. Khan, P. Panini, S. U. Khan, U. A. Rana, H. Andleeb, D. Chopra, S. Hameed and J. Simpson, *Cryst. Growth Des.*, 2016, **16**, 1371–1386.

13 A. Bauzá, T. J. Mooibroek and A. Frontera, *CrystEngComm*, 2016, **18**, 10–23.

14 (*a*) A. D. Martin, J. Britton, T. L. Easun, A. J. Blake, W. Lewis and M. Schroder, *Cryst. Growth Des.*, 2015, **15**, 1697–1706; (*b*) A. D. Martin, K. J. Hartlieb, A. N. Sobolev and C. L. Raston, *Cryst. Growth Des.*, 2010, **10**, 5302–5306; (*c*) A. Tarahhomi, M. Pourayoubi, J. A. Golen, P. Zargaran, B. Elahi, A. L. Rheingold, L. Ramírez and T. Mancilla Percino, *Acta Crystallogr., Sect. B: Struct. Sci., Cryst. Eng. Mater.*, 2013, **69**, 260–270; (*d*) Z. Yousefi, H. Eshtiagh-Hosseini, A. Salimi and A. Janiak, *J. Mol. Struct.*, 2015, **1083**, 460–470.

15 *Oxford Diffraction, CrysAlis PRO*, Oxford Diffraction Ltd, Yarnton, England, 2011.

16 L. J. Bourhis, O. V. Dolomanov, R. J. Gildea, J. A. Howard and H. Puschmann, *Acta Crystallogr., Sect. A: Found. Adv.*, 2015, **71**, 59–75.

17 G. M. Sheldrick, *Acta Crystallogr., Sect. A: Found. Crystallogr.*, 2007, **64**, 112–122.

18 O. V. Dolomanov, L. J. Bourhis, R. J. Gildea, J. A. Howard and H. Puschmann, *J. Appl. Crystallogr.*, 2009, **42**, 339–341.

19 Y. Zhao and D. G. Truhlar, *Theor. Chem. Acc.*, 2008, **120**, 215–241.

20 (*a*) S. Grimme, *J. Comput. Chem.*, 2004, **25**, 1463–1473; (*b*) S. Grimme, *J. Comput. Chem.*, 2006, **27**, 1787–1799; (*c*) S. Grimme, J. Antony, S. Ehrlich and H. Krieg, *J. Chem. Phys.*, 2010, **132**, 154104.

21 S. F. Boys and F. D. Bernardi, *Mol. Phys.*, 1970, **19**, 553–566.

22 M. W. Schmidt, K. K. Baldridge, J. A. Boatz, S. T. Elbert, M. S. Gordon, J. H. Jensen, S. Koseki, N. Matsunaga, K. A. Nguyen, S. Su, T. L. Windus, M. Dupuis and J. A. Montgomery, *J. Comput. Chem.*, 1993, **14**, 1347–1363.

23 (*a*) J. J. McKinnon, F. P. A. Fabbiani and M. A. Spackman, *Cryst. Growth Des.*, 2007, **7**, 755–769; (*b*) M. A. Spackman, J. J. McKinnon and D. Jayatilaka, *CrystEngComm*, 2008, **10**, 377–388; (*c*) M. A. Spackman and D. Jayatilaka, *CrystEngComm*, 2009, **11**, 9–32.

24 S. K. Wolff, D. J. Grimwood, J. J. McKinnon, M. J. Turner, D. Jayatilaka and M. A. Spackman, *CrystalExplorer (Version 3.1)*, University of Western Australia, 2012.

25 P. K. Chattaraj, R. Das, S. Duley and S. Giri, *Chemical Modelling: Applications and Theory*, 2011, vol. 8, p. 45.

26 (*a*) J. F. Galan, C. N. Tang, S. Chakrabarty, Z. Liu, G. Moyna and V. Pophristic, *Phys. Chem. Chem. Phys.*, 2013, **15**, 11883; (*b*) E. Sánchez-García, A. Mardyukov, M. Studentkowski, L. A. Montero and W. Sander, *J. Phys. Chem. A*, 2006, **110**, 13775–13785; (*c*) D. Kaur and S. Khanna, *Struct. Chem.*, 2011, **23**, 755–764; (*d*) D.-M. Huang, Y.-B. Wang, L. M. Visco and F.-M. Tao, *Chem. Phys. Lett.*, 2005, **407**, 222–226.

27 M. G. Smith, R. P. Forbes and A. Lemmerer, *Cryst. Growth Des.*, 2015, **15**, 3813–3821.

28 (*a*) T. Steiner, *Angew. Chem., Int. Ed.*, 2002, **41**, 48–76; (*b*) R. Bishop, *CrystEngComm*, 2015, **17**, 7448–7460.

